JOURNAL OF Applied Polymer SCIENCE

Ablation properties of aluminum silicate ceramic fibers and calcium carbonate filled silicone rubber composites

Cheng Zhou, Lin Yu, Wei Luo, Yang Chen, Huawei Zou, Mei Liang
State Key Lab of Polymer Materials Engineering, Polymer Research Institute of Sichuan University, Chengdu 610065, People's Republic of China
Correspondence to: H. Zou (E-mail: hwzou@163.com) and M. Lang (E-mail: liangmeiww@163.com)

ABSTRACT: The ablative performance of aluminum silicate ceramic fiber (ASF) and calcium carbonate ($CaCO_3$) filled silicone rubber composites prepared through a two-roll mill was examined. The properties of the composites were investigated by thermogravimetry, thermal conductivity measurements, and oxyacetylene torch testing. After the material was burnt, the structure and composition of the char were analyzed by Fourier transform infrared spectroscopy, X-ray diffraction, and scanning electron microscopy (SEM). The results of the ablation test showed that the ablation resistance improved greatly in an appropriate filler scope. Combined with SEM, it was proven that a firm, dense, and thermal insulation layer, which formed on the composites surface during the oxyacetylene torch test, was a critical factor in determining the ablation properties. Thermogravimetric analysis revealed that the thermal stability of the composites was enhanced by the incorporation of ASF and $CaCO_3$. The thermal conductivity measurements showed that the silicone rubber composites had a very low thermal conductivity ranging from 0.206 to 0.442 W m^{-1} K^{-1}; this significantly prevented heat from transferring into the inner matrix at the beginning of the burning process. The proportion of 20/40 phr (ASF/$CaCO_3$) was optimum for improving the ablation resistance of the silicone rubber composites. © 2014 Wiley Periodicals, Inc. J. Appl. Polym. Sci. **2015**, *132*, 41619.

KEYWORDS: composites; rubber; thermal properties; thermogravimetric analysis

Received 13 July 2014; accepted 9 October 2014
DOI: 10.1002/app.41619

INTRODUCTION

As the rapid development of rocket and missile technology, ablation-resistant polymeric composites have been widely used in the aerospace industry.[1–3] A lot of studies have been involved in ablative materials, but most of them have concentrated on phenolic materials, C/C composites, and some polyester materials.[4–6] Compared with these materials, flexible ablation-resistant materials not only have excellent thermal stability, but they also possess good structure designability.

Silicone rubber is considered one of the most important flexible ablation-resistant matrix for two reasons: (1) the —Si—O— bonds in the backbone has excellent thermal stability at 400°C and high residual yield in a nitrogen atmosphere,[7] and (2) they have extremely high backbone flexibility and very low glass-transition temperatures,[8–11] around −120°C. Unfortunately, silicone rubber only forms a very weak powdered char on the surface and can be removed by burning; thus, it displays inferior anti-ablation properties.[12] Therefore, fillers such as clay, carbon fibers (CFs), silicate, SiC, ZrC, and ZrO_2 have attracted considerable interest over the past decade in increasing the ablation properties of silicone rubber.[12–16] Although powder or granules can make ceramic layer dense, the ceramic layer is also easily blown away in the process of flame scouring, and this greatly limits their applications at severely high temperatures. So, it has been found that silicone rubber filled with fiber/particle compounds can form a dense, firm char surface; this is considered to enhance the ablation resistance of silicone rubber composites. On one hand, fiber can form a necessary support between ceramic layers; this is helpful for increasing the gas flushing resistance. On the other hand, particles improve the compactness of the ceramic layer and increase the hardness and strength.[14]

Typical pure silicone rubber usually has poor thermal conductivities (0.2 W m^{-1} K^{-1}).[17] However, silicone rubber can be made into composites with good thermal conductivities when it is filled with thermally conductive fillers, such as Al_2O_3, graphite, SiC, BN, and ZnO.[18–22]

To our surprise, little research has focused on the ablation resistance of silicone rubber composites filled with a low thermally conductive filler. In other words, researchers have seldom focused on the thermal conductivity of the composites. In fact, the low thermal conductivity of the composites is also important for improving the ablation resistance, especially at the beginning of the ablation process, for example, insulating the heat.

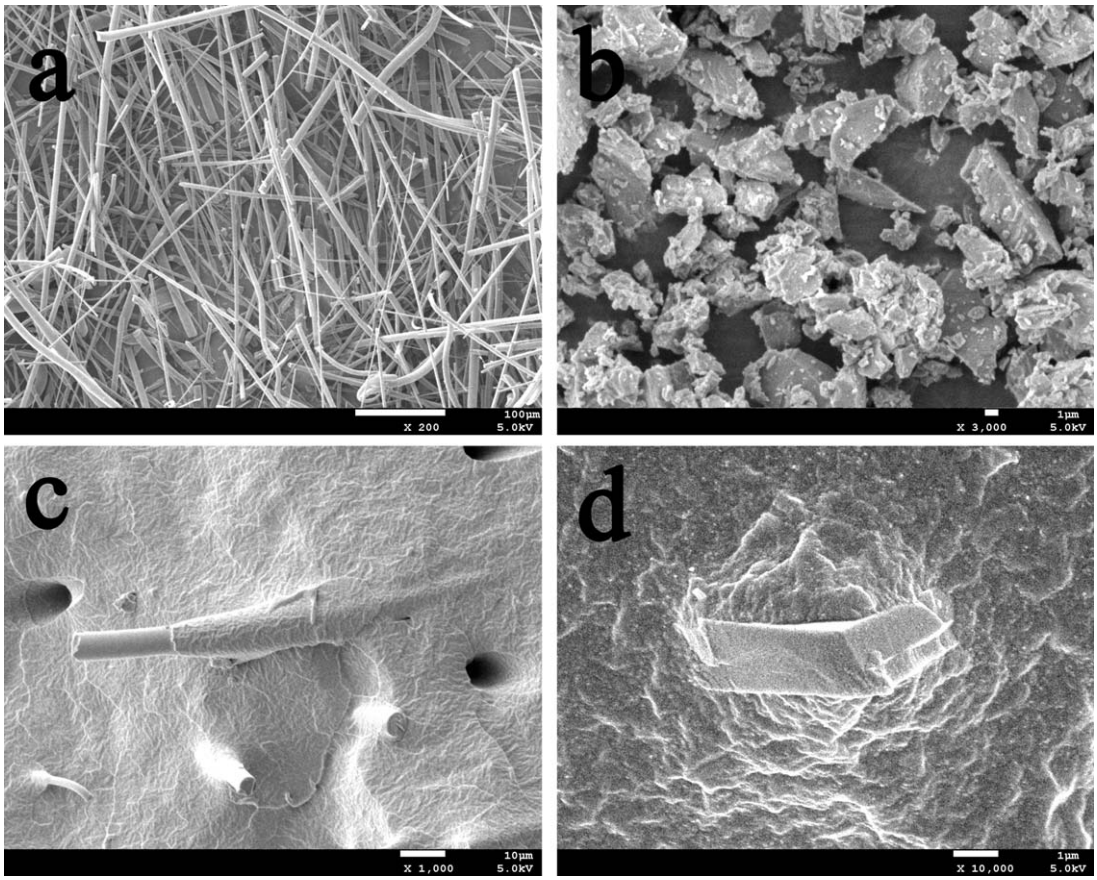

Figure 1. SEM images of the (a) ASF (200×), (b) $CaCO_3$ (3000×), (c) PMVS/ASF (1000×), and (d) PMVS/$CaCO_3$ (10,000×).

In this study, calcium carbonate (thermal conductivity = 2.5 W m^{-1} K^{-1}) and aluminum silicate ceramic fiber (ASF; thermal conductivity: 0.128 W m^{-1} K^{-1}) were selected as a fiber/particle complex filler; this was considered to obtain low thermally conductive silicone rubber and generate a firm and thermal insulating layer after burning. The content of the ASF was fixed at 20 phr for the difficulties in sample processing and the outstanding ablation resistance at this proportion.[23] The effects of the systems on the ablation properties of the composites were analyzed through an ablation test. The morphology, thermal conductivity, and thermal stability of the composites and the components of ceramic layer were also investigated in this research.

EXPERIMENTAL

Materials

The silicone rubber used in this study was polymethylvinylsiloxane (PMVS), with an average molecular weight of about 640,000 g/mol and a vinyl content of 0.16%/mol, made by Wynca Chemical (China). Fumed silica (SiO_2, Degussa, Germany) was used to enhance the breaking strength and tenacity of the composites. Dicumyl peroxide, a curing agent, was obtained from Chengdu Kelong Chemical Reagents Factory (China). ASF was supplied by Nanjing Suowo Technology (China). Calcium carbonate ($CaCO_3$) was purchased from Chengdu Stars Phosphate Factory (China). The morphology of ASF, $CaCO_3$, PMVS/ASF, and PMVS/$CaCO_3$ are clearly shown in Figure 1. ASF clearly showed a typical fiber morphology, whereas $CaCO_3$ exhibited a powder shape. In addition, they were well bonded with the matrix.

Sample Preparation

The composites were prepared with a two-roll mill at ambient temperature. Silicone rubber was added first, and then, relevant fillers were added in turn. ASF was introduced as the last component to reduce the possibility of a breakdown of the fibers during mixing. The whole process lasted 5 min and then continued for another 5 min at 40°C after the curing agent was added. The samples used for the measurements were cured and compression-molded at 175°C for 15 min under a pressure of 10 MPa and then cooled under this pressure to room temperature. The secondary vulcanization process was carried out at 200°C in an airflow drier for 2 h.

For simplicity, composites containing ASF and $CaCO_3$ were designated as $S_{0/0}$, $S_{20/0}$, $S_{20/20}$, $S_{20/40}$, $S_{20/60}$, and $S_{20/80}$. The additive amounts of ASF/$CaCO_3$ used to prepare the silicone rubber composites in this study are presented in Table I. The additive amount of dicumyl peroxide was fixed at 1 phr in all of the samples.

Characterization

Ablation Test. Ablation experiments were conducted with an oxygen–acetylene torch (oxyacetylene). The samples were

Table I. Amounts of ASF/$CaCO_3$ in the Silicone Rubber Composites

Sample	ASF (phr)[a]	$CaCO_3$ (phr)
$S_{0/0}$	0	0
$S_{20/0}$	20	0
$S_{20/20}$	20	20
$S_{20/40}$	20	40
$S_{20/60}$	20	60
$S_{20/80}$	20	80

[a] phr, parts per hundred of silicone rubber by weight.

compression-molded with dimensions of 40 × 40 ×7.5 mm^3. The flow rates of oxygen (O_2) and acetylene (C_2H_2) were 0.30 and 0.24 m^3/h, respectively. The specimen was placed vertically to the flame direction in air. The distance between the nozzle tip of the oxyacetylene gun and the front surface of the specimen was 10 mm, and the inner diameter of the tip was 1.6 mm. The surface temperature of the samples was about 1800°C and was monitored by an optical pyrometer. The ablation duration for each sample was deliberately fixed at 60 s. The line ablation rate (R_d; mm/s) was calculated with the following equation:

$$R_d = \frac{\Delta d}{t} = \frac{d_1 - d_2}{t}$$

where Δd is the change of specimen thickness before and after ablation test, d_1 is the original thickness of the specimen before the ablation treatment (mm), d_2 is the resulting thickness after the ablation treatment (mm), and t is the ablation time during the fire treatment process (s). Samples with lower R_d values exhibited better ablation-resistant properties. The process of the oxyacetylene ablation test is shown in Figure 2.

Morphological Study

The morphology of the composites after ablation process was characterized by scanning electron microscopy (SEM; JSM-5900, JEOL, Tokyo, Japan) instrument. The fired surfaces of the samples were coated with gold to enhance image resolution and to prevent electrostatic charging.

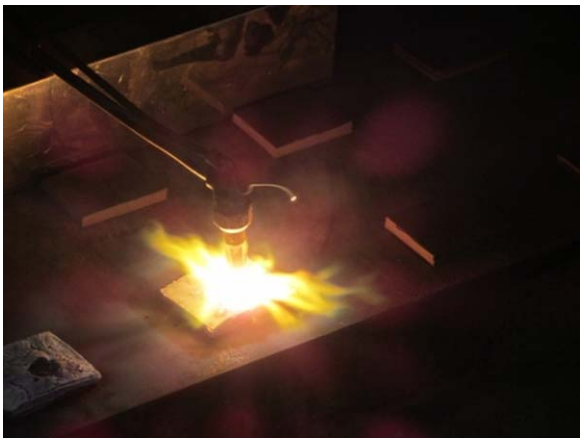

Figure 2. Photograph of the oxyacetylene ablation process. [Color figure can be viewed in the online issue, which is available at wileyonlinelibrary.com.]

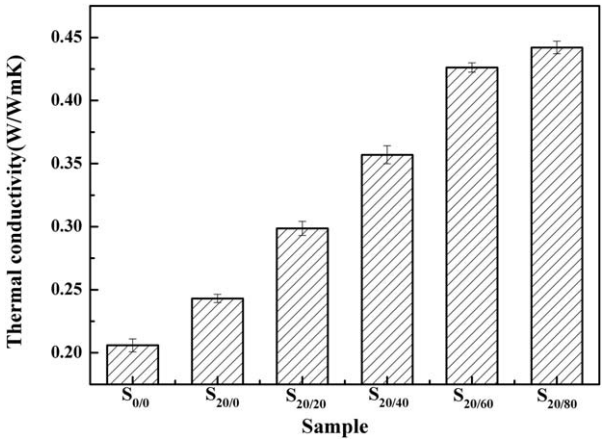

Figure 3. Thermal conductivity versus the content of ASF/$CaCO_3$.

Thermogravimetric Analysis (TGA)

TGA was conducted on a thermogravimetric analyzer (TG 209F1 Iris, Netzsch, Germany) to investigate the thermal stability of the samples under dry nitrogen gas with a flow rate of 60 mL/min. The samples were heated at a rate of 10°C/min, and the relative mass loss of the samples was recorded from 40 to 800°C.

X-ray Diffraction (XRD) Analysis

Wide-angle XRD scans of the composites after the ablation treatment were carried out on a D/MAX-III X-ray diffractometer (DY1291, Philips, Holland) with a wavelength of 0.1542 nm of Cu Kα at a generator voltage of 40 kV and a generator current of 35 mA. The scans were conducted in the 2θ angle range from 2 to 80° with a speed of 9°/min.

Fourier Transform Infrared (FTIR) Measurement

FTIR spectra were obtained in the range 4000–400 cm^{-1} with a resolution of 1 cm^{-1} with a Nicolet iZ10 FTIR spectrophotometer (Nicolet) with a potassium bromide (KBr) pellet technique. The sample was scanned from 4000 to 600 cm^{-1}.

TGA–FTIR Spectroscopy

A thermogravimetric analyzer (Mettler-Toledo) coupled to an FTIR spectrophotometer (Thermo-Nicolet) was used to investigate the mass loss of $CaCO_3$ and the online formation of gas products. About 20 mg of the $CaCO_3$ sample was placed into the furnace and heated from 40 to 800°C at a heating rate of 10°C/min under a nitrogen flow of 40 mL/min to maintain an inert atmosphere. The scanning range of FTIR spectroscopy was set from 4000 to 800 cm^{-1} with a resolution of 8 cm^{-1}.

Thermal Conductivity Measurement

Thermal conductivity measurement of the composites was carried out by a thermal constant analyzer (Hot Disk TPS 2500, Sweden) with a certain electrical power and corresponding measuring time exerted on the prepared samples. The hot disk sensor was placed tightly between two pieces of the prepared samples. The sensor functioned as both a heat source and a temperature sensor. The experimental data of both samples were collected at the same time, and the reported thermal conductivity demonstrated the average value of both samples. The thermally conductive value

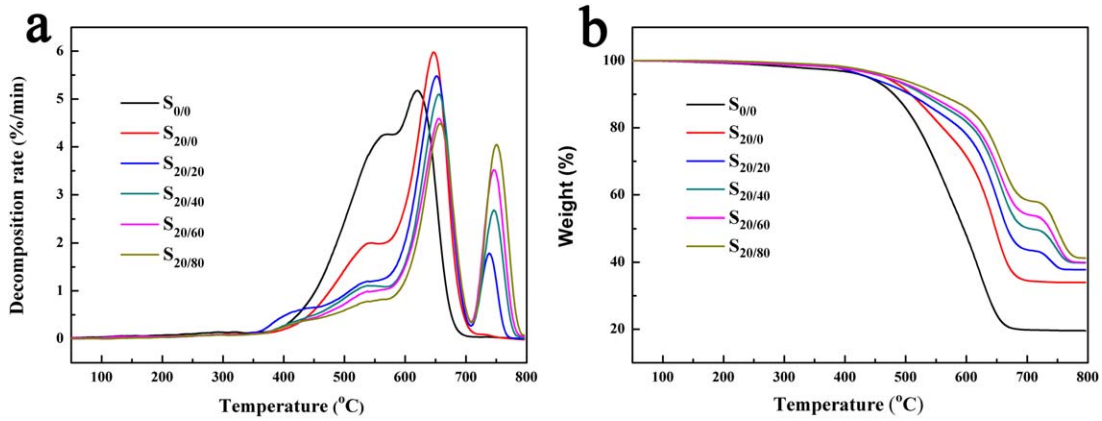

Figure 4. Derivative thermogravimetry curves and TGA curves of six types of silicone rubber composites. [Color figure can be viewed in the online issue, which is available at wileyonlinelibrary.com.]

acquired was a comprehensive value of all directions, not just the in-plane or through-plane direction

RESULTS AND DISCUSSION

Thermal Conductivity of the Composites

The effect of the loading concentration of ASF/$CaCO_3$ on the thermal conductivity of the silicone composites is shown in Figure 3. The thermal conductivity of the composites increased with the ASF loading from 0 to 20 phr but increased faster after $CaCO_3$ was incorporated; this was mainly ascribed to the lower thermal conductivity of ASF at 0.128 W m^{-1} K^{-1}. When the content of $CaCO_3$ increased from 0 to 60 phr, the thermal conductivity enlarged almost linearly. With a further increase in the $CaCO_3$ loading, thermally conductive networks formed, and the filler no longer played a vital role in enhancing the thermal conductivity, whereas the packing structure of the filler and defects introduced during the process became the main factors that impaired the overall thermal conductivity of the composites.[24] In light of these factors, the thermal conductivity increased rather slowly at a high loading fraction of $CaCO_3$ from 60 to 80 phr.

A very low thermal conductivity of the silicone composites was obtained and ranged from 0.206 to 0.442 W m^{-1} K^{-1}; this was much lower than the value reported by Zhou *et al.*[20] They reported a value of 1.48 W m^{-1} K^{-1} in 50 vol % hybrid Si_3N_4 particle reinforced silicone rubber composites. This value was also much lower than the value reported by Wang *et al.*;[25] they reported a value of 2 W m^{-1} K^{-1} with increasing total volume fraction of the filler (α-Al_2O_3, SiC) with adequate filler size distributions in room-temperature-vulcanized silicone rubber. The low thermally conductive surface of silicone composites effectively prevented heat from transferring into the inner layer. This improved the thermal stability and ablation resistance performance of the composites.

Thermal Degradation Behavior of the Composites

The derivative thermogravimetry and TGA curves of all the samples under nitrogen atmosphere are shown in Figure 4.

As shown in Figure 4(a), the thermal degradation of pure PMVS took two mass loss steps. The first step was attributed to the thermal degradation of the methyl branches occurring between 380 to 580°C, which produced methane and other organic gases. The second step might have been due to the depolymerization of the siloxane chains occurring between 580 and 700°C by the production of cyclic trimers or tetramers.[26,27]

Unlike pure PMVS, the main decomposition reaction and weight loss of the composites occurred in the second process.

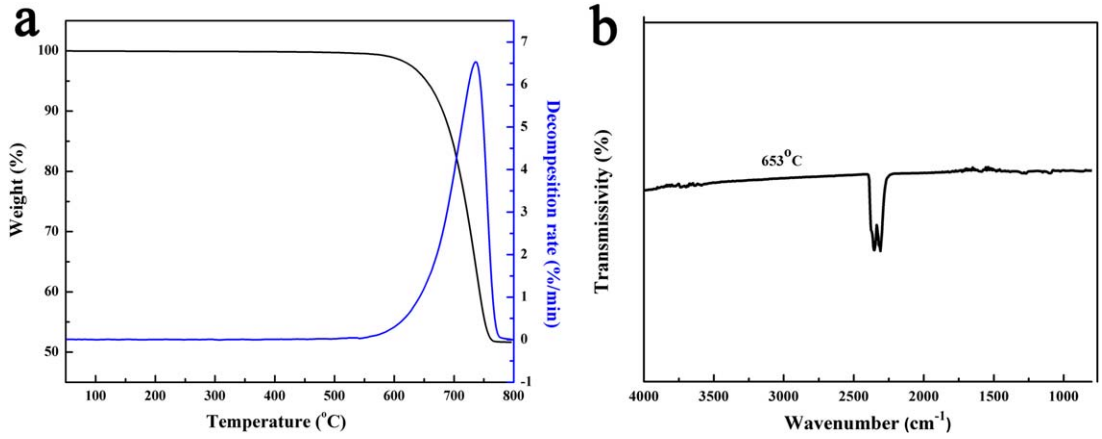

Figure 5. Thermogravimetry–FTIR analysis curves for $CaCO_3$. [Color figure can be viewed in the online issue, which is available at wileyonlinelibrary.com.]

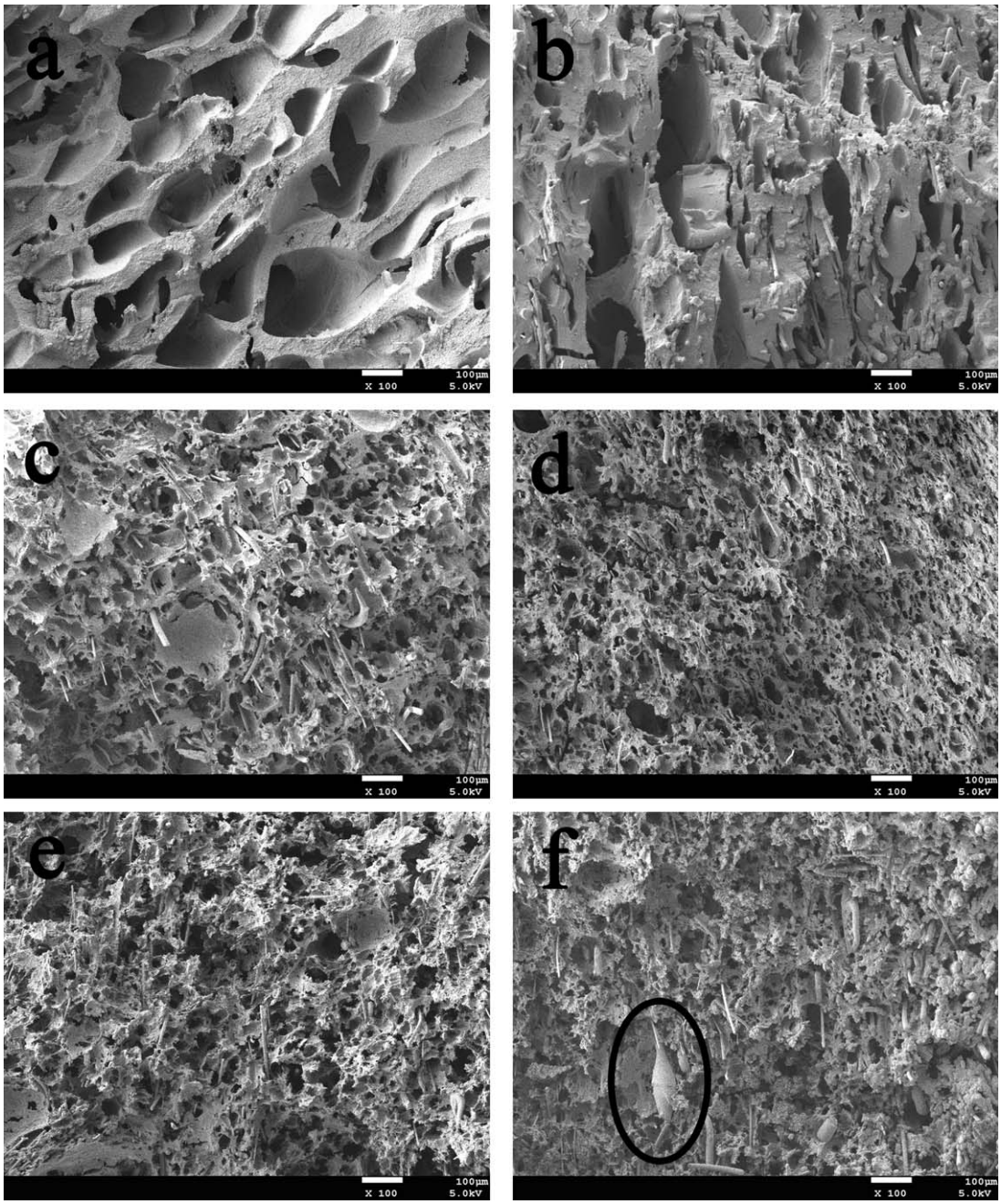

Figure 6. Morphologies of the ablated composites with various loading fractions of ASF/$CaCO_3$ at 100×: (a) $S_{0/0}$, (b) $S_{20/0}$, (c) $S_{20/20}$, (d) $S_{20/40}$, (e) $S_{20/60}$, and (f) $S_{20/80}$.

The TGA results [Figure 4(b)] revealed that as the content of ASF and $CaCO_3$ increased, the temperature at which the 5 wt % mass loss of pure PMVS and the composites occurred was raised from 438 to 481°C. There was also a tremendous increase in the residual yield at 800°C; this increased from 19.6 to 41.2%. These results show that the thermal stability of the silicone rubber composites was improved effectively. This was attributed to two reasons. First, the fillers were more thermally stable than the matrix. Second, some siloxane bonds may have been opened by heat and macromolecular free radicals formed. The chain reactions of these macromolecular free radicals could be ended on the fillers. The interactions between the fillers and silicone rubber led to an increase in the physical and chemical crosslinking points.[18,20,28]

When the $CaCO_3$ load increased, the residual yield at 800°C increased, and the decomposition rate decreased accordingly. This was due to the low thermal conductivity of $CaCO_3$, which geared down the heat-transfer rate. As shown in Figure 5(a), the decomposition of pure $CaCO_3$ mainly occurred at about 600–800°C, and the residual yield was about 50%; this was in agreement with the added residual yield between the samples containing or not containing $CaCO_3$. These all demonstrated

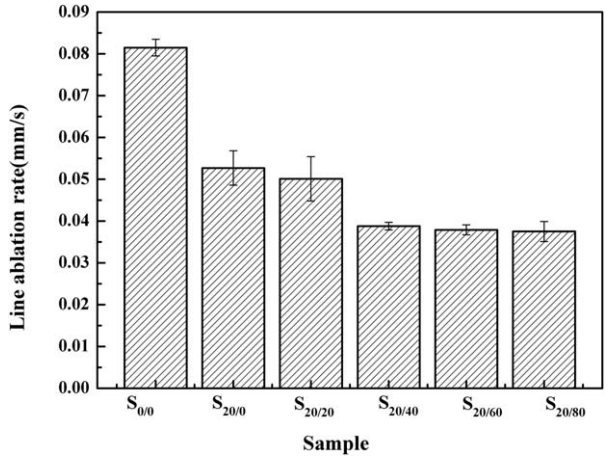

Figure 7. R_d values of the composites with different loadings of ASF/$CaCO_3$.

that the reaction of $CaCO_3$ itself was responsible for the slight weight loss observed from 710 to 790°C. Furthermore, the IR absorption peak of CO_2 [Figure 5(b)] at 2310.5 and 2354.3 cm^{-1} indicated that $CaCO_3$ would decompose to CaO and CO_2 in the ablation process. The former could attenuate the concentration of the oxygen and combustible gas and provide a flame-retardant effect; the latter could counteract the acid product and protect the substrate.

Burnt Morphology and Ablation Properties of the Composites

Figure 6 shows the morphology of the composites with different contents of filler after ablation. The representative micrograph [Figure 6(a–d)] shows that the size of the holes in the ceramic layer was reduced and the hardness of the ceramic layer was enhanced after the addition of ASF/$CaCO_3$ in the composites. These results suggest that, first, ASF could form necessary support between the ceramic layers; this was helpful for increasing the gas flushing resistance. Second,

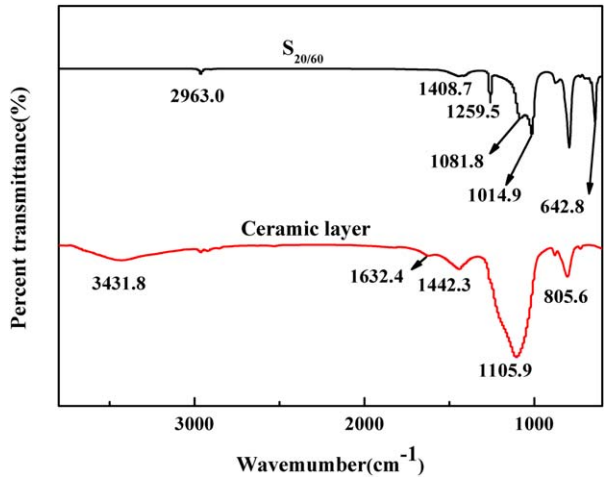

Figure 8. FTIR spectra for the virgin and ceramic layers of $S_{20/40}$. [Color figure can be viewed in the online issue, which is available at wileyonlinelibrary.com.]

$CaCO_3$ improved the compactness of the ceramic layer, increasing the hardness and strength. However, Figure 6(d–f) demonstrated that the density of the ceramic layer changed little with the percentage of $CaCO_3$ at 40, 60, and 80 phr. The reason may have been that the decomposition of $CaCO_3$ itself slowed down the increase of the amount of the residue yield. Moreover, interconnecting physical networks nearly formed in the composites with the content of $CaCO_3$ at 40 phr; this led to a rapid growth of the ablation resistance of the composite system. Specifically, it is shown in Figure 6(f) that the newly formed ellipsoids should have been $CaSiO_3$; this came from the reaction between the fillers and the matrix during the ablation process.

As shown in Figure 7, the linear ablative rate decreased with increasing concentration of ASF/$CaCO_3$. After the addition of 20/40 phr of ASF/$CaCO_3$, the linear ablation rate was only 0.0388 mm/s; this was much lower than the 0.0815 mm/s rate of pure specimen. The value of the ablation rate was also lower than the results reported by Yang *et al.*[29] They reported a value of 0.0472 mm/s for CF/SiO_2 filled polydimethylsiloxane/polydimethylphenylsiloxane ablative composites at a CF/SiO_2 loading fraction of 15/30 phr. The lower thermally conductive surface and dense ceramic layer formed during the ablation process were believed to be responsible for the lower linear ablative rate. However, when the content of $CaCO_3$ was increased further, the linear ablative rate did not fulfill this expectation. We believed that the composites with 40 phr $CaCO_3$ could form a dense layer of protection; this is clearly shown in Figure 6. This agreed with the thermal conductivity test, in which the thermally conductive network was formed at 40 phr of $CaCO_3$; going on to add the additional amount of $CaCO_3$ did not significantly improve the thermal conductivity of the composites. This relationship is a well-known phenomenon for composites, and this indicates physical network formation by the inorganic fillers.[30,31]

Components and Microstructure of the Ablated Surface

The virgin layer (before ablation) and the ceramic layer of the composites were identified by FTIR spectroscopy and XRD, as shown in Figures 8 and 9.

The FTIR peaks assigned to the vibrations of the methyl groups (at 2963.0, 1408.7, 1259.5, and 1014.9 cm^{-1})[29] disappeared in the ceramic layer; this suggested that scission of the Si—C bonds in the silicone rubber side chains occurred. Meanwhile, the weakened sign for Si—C at 805.6 cm^{-1} was ascribed to the destruction of the network formed by the interrelating vinyl groups. This resulted in the crack of the Si—C bond. The FTIR peak situated at 1632.4 cm^{-1} in the ceramic layer belonged to the stretching vibrations of C=C and indicated the formation of residual carbon in the layer. The peaks observed at 1081.8 cm^{-1} were attributed to the typical peak for the Si—O bond existing in trimers, tetramers, SiO_2, ASF, and the matrix. In the ceramic layer, the peak at 3431.8 cm^{-1} was assigned to the vibrations of the hydroxyl (—OH) groups. The reasons may have been that on one hand, the formation of SiO_2 during condensation[26] produced hydroxyl groups, as shown in the following reaction:

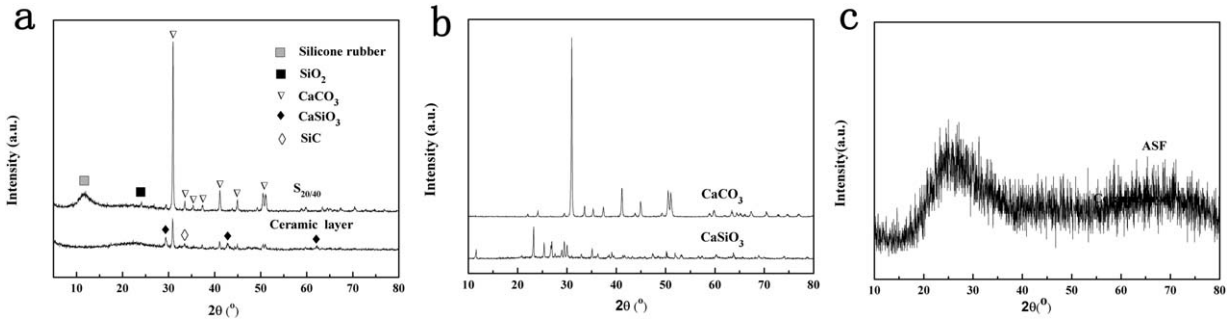

Figure 9. XRD patterns of the materials: (a) virgin and ceramic layers of $S_{20/40}$, (b) $CaCO_3$ and $CaSiO_3$, and (c) ASF.

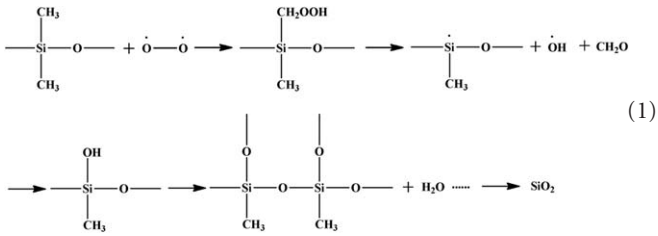

(1)

On the other hand, the porous char layer tended to absorb the moisture and, thus, displayed the typical peak for hydroxyl groups.

XRD experiments were carried out to investigate the crystal structure behavior of the ceramic layer of $S_{20/40}$. For comparison, the XRD patterns of the virgin layers of $S_{20/40}$, $CaCO_3$, ASF, and $CaSiO_3$ were also examined. The characteristic peaks observed at 11.8 and 23.8° in the ceramic layer [Figure 9(a)] were attributed to silicone rubber and SiO_2, respectively.[29] A weak broad convex was observed in the XRD patterns of the ablated surface of the composites [Figure 9(c)] from 20 to 28°; this suggested that the compound ASF still existed in the layer. Notably, the characteristic peak of silicone rubber vanished from the ceramic layer; this suggested the decomposition of silicone rubber after ablation [Figure 9(a)]. The XRD patterns of the ceramic layer did not exhibit the peaks of residual carbon ($2\theta = 25.5°$);[29,32] the reasons could have been that the peaks were covered by the broad peaks of ASF.

Because ASF still existed in the ablated composites because of its excellent temperature resistance, the chemical interaction between the fillers we used and the silicone rubber mainly occurred among $CaCO_3$, SiO_2, and silicone rubber. The XRD patterns of the ceramic layer after ablation did not display the diffraction peaks of $CaCO_3$ but showed the patterns of $CaSiO_3$ instead [Figure 9(a,b)]. Combined with thermogravimetry–FTIR analysis, this indicated that $CaCO_3$ produced CaO and CO_2 during the process of ablation. Furthermore, at higher temperatures, CaO reacted with SiO_2, which came from the thermal degradation of PMVS, and then produced $CaSiO_3$.[33] The calcium silicate may have been formed according to the reaction sequence in eqs. (2)–(4):

$$\text{PMVS} \rightarrow \text{SiO}_2 + \text{VOC} \uparrow (> 500^\circ\text{C}) \quad (2)$$

$$\text{CaCO}_3 \rightarrow \text{CaO} + \text{CO}_2 \uparrow (> 600^\circ\text{C}) \quad (3)$$

$$\text{CaO} + \text{SiO}_2 \rightarrow \text{CaSiO}_3 (> 600^\circ\text{C}) \quad (4)$$

The relatively low temperature allowed the formation of a small amount of SiC, as evidenced by the peak located around 33.6° [Figure 9(a)].[34] The SiC may have been generated according to the following mechanism:

$$\text{SiO}_2 + \text{C (residual carbon)} \rightarrow \text{SiC} + \text{CO} \uparrow \quad (5)$$

$$\text{SiO}_2 + \text{CO} \rightarrow \text{SiC} + \text{CO}_2 \uparrow \quad (6)$$

In addition, $CaSiO_3$ and SiC were both high-temperature-resistant minerals that could be expected to improve the ablation resistance of the composite systems.

CONCLUSIONS

In this study, we devised highly ablation-resistant silicone rubber composites filled with low thermally conductive ASF and $CaCO_3$ through a blending process. A linear ablation rate of 0.0375 mm/s was achieved for the silicone composites at its maximum filler loading of 20/80 phr, and this linear ablation rate was approximately 52.99% lower than that of the virgin PMVS.

The linear ablation rate of the composites decreased with increasing ASF/$CaCO_3$ content; this was mainly ascribed to the dense surface layer formed during the heat treatment and the low thermally conductive surface of the materials. SEM indicated that a dense and firm ceramic layer formed after the addition of ASF and $CaCO_3$. TGA revealed that the thermal stability of the ASF- and $CaCO_3$-modified silicone rubber improved compared with that of the neat rubber. In the ablation process, $CaCO_3$ decomposed to CaO and CO_2. Then, $CaSiO_3$ was formed at high temperatures through a reaction between CaO and SiO_2.

In a word, the results revealed that the addition of ASF and $CaCO_3$ was crucial to the enhancement of the ablation resistance for the silicone rubber composites. When ASF was fixed at an optimized content of 20 phr, optimum ablation properties were observed at a proportion of 40 phr for $CaCO_3$ in the rubber composites.

ACKNOWLEDGMENTS

The authors thank the National Natural Science Foundation of China (contract grant number 51273118) and the Science and Technology Pillar Program of Sichuan (contract grant number 2013FZ0006) for financial support and the Analytical and Testing Center of Sichuan University for providing SEM and XRD measurements.

REFERENCES

1. Natali, M.; Monti, M.; Puglia, D.; Kenny, J. M.; Torre, L. *Compos. A* **2012**, *43*, 174.
2. Vaia, R. A.; Price, G.; Ruth, P. N.; Nguyen, H. T.,; *Lichtenhan. Appl. Clay Sci.* **1999**, *15*, 67.
3. Bahramian, A. R.; Kokabi, M. *J. Hazard. Mater.* **2009**, *166*, 445.
4. Henderson, J. B.; Wiecek, T. E. *J. Compos. Mater.* **1987**, *21*, 373.
5. McManus, H. L.; Springer, G. S. *J. Compos. Mater.* **1992**, *26*, 206.
6. Klett, J. W.; Ervin, V. J.; Edie, D. D. *Compos. Sci. Technol.* **1999**, *59*, 593.
7. Hanu, L. G.; Simon, G. P.; Cheng, Y. B. *Polym. Degrad. Stab.* **2006**, *91*, 1373.
8. Chen, D.; Yi, S.; Fang, P.; Zhong, Y.; Huang, C.; Wu, X. *React. Funct. Polym.* **2011**, *71*, 502.
9. Wang, C.; Ren, J. X.; Liu, Y.; Hao, W. Q.; Yang, J. X. *Key Eng. Mater.* **2014**, *575*, 427.
10. Xu, Q.; Pang, M.; Zhu, L.; Zhang, Y.; Feng, S. *Mater. Des.* **2010**, *31*, 4083.
11. Lötters, J. C.; Olthuis, W.; Veltink, P. H.; Bergveld, P. *J. Micromech. Microeng.* **1997**, *7*, 145.
12. Soo Kim, E.; Lee, T. H.; Shin, S. H.; Yoon, J. S. *J. Appl. Polym. Sci.* **2011**, *120*, 831.
13. Kim, E. S.; Kim, E. J.; Shim, J. H.; Yoon, J. S. *J. Appl. Polym. Sci.* **2008**, *110*, 1263.
14. Yang, D.; Zhang, W.; Jiang, B. Z.; Guo, Y. *Compos. A* **2013**, *44*, 70.
15. Mansouri, J.; Burford, R. P.; Cheng, Y. B.; Hanu, L. *J. Mater. Sci.* **2005**, *40*, 5741.
16. Mansouri, J.; Burford, R. P.; Cheng, Y. B. *Mater. Sci. Eng. A* **2006**, *425*, 7.
17. Zhou, W.; Qi, S.; Tu, C.; Zhao, H.; Wang, C.; Kou, J. *J. Appl. Polym. Sci.* **2007**, *104*, 1312.
18. Sim, L.; Ramanan, S. R.; Ismail, H.; Seetharamu, K. N.; Goh, T. *J. Thermochim. Acta* **2005**, *430*, 155.
19. Mu, Q.; Feng, S. *Thermochim. Acta* **2007**, *462*, 70.
20. Zhou, W.; Wang, C.; An, Q.; Ou, H. *J. Compos. Mater.* **2008**, *42*, 173.
21. Kemaloglu, S.; Ozkoc, G.; Aytac, A. *Thermochim. Acta* **2010**, *499*, 40.
22. Mu, Q.; Feng, S.; Diao, G. *Polym. Compos.* **2007**, *28*, 125.
23. Yu, L.; Zhou, S.; Zou, H.; Liang, M. *J. Appl. Polym. Sci.* **2013**, DOI:10.1002/app.39700.
24. Zhou, S.; Yu, L.; Song, X.; Chang, J.; Zou, H.; Liang, M. *J. Appl. Polym. Sci.* **2013**, DOI:10.1002/app.39596.
25. Wang, Q.; Gao, W.; Xie, Z. *J. Appl. Polym. Sci.* **2003**, *89*, 2397.
26. Oyumi, Y. *J. Polym. Sci. Part A: Polym. Chem.* **1998**, *36*, 233.
27. Radhakrishnan, T. S. *J. Appl. Polym. Sci.* **1999**, *73*, 441.
28. Zhang, J.; Feng, S.; Ma, Q. *J. Appl. Polym. Sci.* **2003**, *89*, 1548.
29. Yang, D.; Zhang, W.; Jiang, B. *Ceram. Int.* **2013**, *39*, 1575.
30. Kasgoz, A.; Akın, D.; Durmus, A. *Polym. Eng. Sci.* **2012**, *52*, 2645.
31. Pötschke, P.; Fornes, T. D.; Paul, D. R. *Polymer* **2002**, *43*, 3247.
32. Gumula, T.; Blazewicz, S. *Ceram. Int.* **2013**, *39*, 3795.
33. Hermansson, A.; Hjertberg, T.; Sultan, B. A. *Fire Mater.* **2003**, *27*, 51.
34. Ryu, Z. Y.; Zheng, J. T.; Wang, M. Z.; Zhang, B. *J. Carbon* **2001**, *39*, 1929.